Total internal reflection fluorescence lifetime and anisotropy screening of cell membrane dynamics

Thomas Bruns
Hochschule Aalen, Institut für Angewandte Forschung
Beethovenstr. 1
73430 Aalen, Germany

Wolfgang S. L. Strauss
Institut für Lasertechnologien in der Medizin und Meßtechnik an der Universität Ulm
Helmholtzstr. 12
89081 Ulm, Germany

Herbert Schneckenburger
Hochschule Aalen, Institut für Angewandte Forschung
Beethovenstr. 1
73430 Aalen, Germany
and
Institut für Lasertechnologien in der Medizin und Meßtechnik an der Universität Ulm
Helmholtzstr. 12
89081 Ulm, Germany

Abstract. A high content screening (HCS) system for fluorescence measurements at surfaces, in particular the plasma membrane of living cells, is described. The method is based on multiple total internal reflections (TIRs) of an incident laser beam within the glass bottom of a microtiter plate such that up to 96 individual samples could be illuminated by an evanescent electromagnetic field. Fluorescence lifetimes and time-resolved fluorescence anisotropies of these samples were assessed. While fluorescence lifetime represents a general measure for the interaction of a marker molecule with its microenvironment, the rotational diffusion time corresponds to the relaxation time of a molecule from a position with a defined orientation into a position with an arbitrary orientation. Thus, time-resolved fluorescence anisotropy reflects the viscosity of the microenvironment, i.e., membrane fluidity in the case of living cells. For all measurements in this study, either human glioblastoma cells incubated with the fluorescent membrane marker NBD-cholesterol or human breast cancer cells expressing a membrane-associating fluorescent protein were used.
 [DOI: 10.1117/1.2953490]

Keywords: high content screening; total internal reflection; fluorescence lifetime; fluorescence anisotropy; living cells; NBD-cholesterol; EYFP-Mem.

Paper 07391SSRR received Sep. 19, 2007; revised manuscript received Apr. 3, 2008; accepted for publication May 2, 2008; published online Jul. 10, 2008.

1 Introduction

For more than 20 years,[1] total internal reflection (TIR) of laser light has been used to study cell-substrate interfaces to get more detailed information on plasma membranes of living cells. When a light beam propagating through a medium of refractive index n_1 (e.g., glass) meets an interface with a second medium of refractive index $n_2 < n_1$ (e.g., cytoplasm), TIR occurs at all angles of incidence Θ that are greater than a critical angle $\Theta_c = \arcsin(n_2/n_1)$. While being totally reflected, the incident beam establishes an evanescent electromagnetic field $\mathbf{E_{ev}}$ that penetrates into the second medium and decays exponentially with the distance z from the interface. According to the relation

$$d = (\lambda/4\pi) \cdot (n_1^2 \sin^2 \Theta - n_2^2)^{-1/2}, \quad (1)$$

penetration depths d between about 60 nm and more than 300 nm are attained for its intensity $I_{ev} \sim E_{ev}$,[2] depending on the wavelength λ and the angle of incidence Θ. Therefore, fluorophores located within or close to the plasma membrane can be examined almost selectively in living cells. So far, total internal reflection fluorescence microscopy (TIRFM) has been applied for measuring the topography of cell-substrate contacts,[1–3] membrane[4] and protein[5] dynamics, membrane-proximal ion fluxes,[6,7] as well as endocytosis and exocytosis.[8–10]

With regard to potential diagnostic or pharmaceutical applications, TIR techniques appear rather promising for measurements of signal transduction, intracellular translocation of molecules, and membrane dynamics. Therefore, screening of a large number of samples is desirable. A first fluorescence reader based on simultaneous TIR of a laser beam on 96 samples of a microtiter plate (high throughput screening, or HTS) was recently described.[11] However, in some cases, e.g., measurements of membrane stiffness and fluidity, additional data of individual samples are needed. Therefore, an optical setup to analyze fluorescence lifetime and fluorescence anisotropy (high content screening, or HCS) was developed and combined with the existing HTS reader system such that individual samples selected by HTS could be examined in detail by HCS. While fluorescence lifetime represents a general measure for the interaction of a marker molecule with its microenvironment, the rotational diffusion time corresponds to the time of rotation of a molecule from a position with a defined orientation into a position with an arbitrary orientation. This reflects directly the viscosity of the microenvironment, i.e., membrane fluidity in the case of living cells.

For basic validation of the system, we used T47D breast cancer cells stably transfected with a plasmid encoding for a plasma membrane-associating yellow fluorescent protein (EYFP-Mem). Further validation of fluorescence lifetime and fluorescence anisotropy was accomplished with the membrane

Address all correspondence to: Herbert Schneckenburger, Hochschule Aalen, Institut für Angewandte Forschung, Beethovenstr. 1, 73430 Aalen, Germany. Tel: +49-7361-576-3401; Fax: +49-7361-576-3318; E-mail: herbert.schneckenburger@htw-aalen.de

1083-3668/2008/13(4)/041317/5/$25.00 © 2008 SPIE

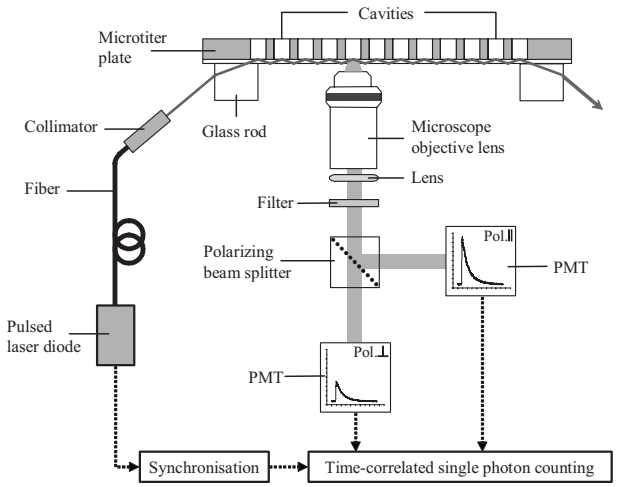

Fig. 1 Experimental setup for fluorescence lifetime and fluorescence anisotropy screening (integration into a HTS has been omitted).

marker 22-(N-(7-nitrobenz-2-oxa-1,3-diazol-4-yl)amino)-23,24-bisnor-5-cholen-3β-ol (NBD-cholesterol) applied to the human glioblastoma cell line U373-MG.

2 Materials and Methods

U373-MG human glioblastoma cells obtained from the European Collection of Cell Cultures (ECACC No. 89081403) were routinely grown in an RPMI 1640 culture medium supplemented with 10% fetal calf serum (FCS), glutamine, and gentamycin at 37 °C and 5% CO_2. After seeding 500 cells/mm^2 within single cavities of a microtiter plate (96-well plate with 6-mm well diameter; Greiner GmbH, Frickenhausen, Germany, with a custom-made glass bottom[11]) and a growth phase of 48 h (to obtain a subconfluent cell monolayer), the cells were incubated for 60 min with Earle's Balanced Salt Solution (EBSS) containing NBD-cholesterol at a concentration of 4 μM. At the end of the incubation time, the cells were washed with EBSS prior to fluorometric measurements. Solutions of 4 μM NBD-cholesterol in EBSS were used for control measurements.

T47D breast cancer cells obtained from the American Type Culture Collection (ATTC, Rockville, Maryland) and stably transfected with the Living colors™ subcellular localization vector pEYFP-Mem (Clontech, Palo Alto, California) were also cultivated in the RPMI 1640 medium supplemented with 10% FCS and antibiotics at 37 °C and 5% CO_2. Again, 500 cells/mm^2 were seeded in single cavities of a microtiter plate and grown for 48 h prior to fluorometric measurements.

The experimental setup developed for fluorescence lifetime and fluorescence anisotropy screening is depicted in Fig. 1. For a light source, we used a picosecond laser diode (LDH-P-C-470 with driver PDL 800-B, PicoQuant GmbH, Berlin, Germany; wavelength 470 nm; pulse width 70 ps; repetition rate 20 MHz; average power 100 μW). Via a polarization maintaining single-mode fiber and a glass rod of rectangular shape, collimated laser light was coupled into the glass bottom of the microtiter plate for excitation of a preselected single row of cavities. In all cases the electric field vector was polarized perpendicular to the plane of incidence. Multiple TIRs occurred within this glass bottom if the angle of incidence Θ was above the critical angle $\Theta_c = 63.9$ deg (resulting from the refractive indices $n_1 = 1.525$ for the glass bottom and $n_2 = 1.37$ for the cells). In the present setup, Θ could be calculated from the distance $s = 9$ mm between two cavities of the plate and the thickness $d = 2$ mm of the glass bottom[11] according to $\Theta = \arctan(s/2d) = 66$ deg. Therefore, the condition of TIR was fulfilled for all cavities, and a penetration depth of the evanescent wave of about 150 nm within the cells was calculated according to Eq. (1). Due to the Gaussian laser beam profile (beam diameter 700 μm), the illumination spot on each cavity of the microtiter plate was of elliptical shape with an area of about 1 mm^2. The exciting laser light was coupled out of the glass bottom by a second glass rod to avoid uncontrolled reflections.

Fluorescence arising from about 2000 cells of each cavity was collected by a detection unit consisting of a microscope objective lens with 10× magnification (numerical aperture NA = 0.30), an additional focusing lens ($f = 25$ mm), and a long-pass filter for $\lambda \geqslant 515$ nm. After passing a polarizing beamsplitter, fluorescence polarized parallel $[I_{\parallel}(t)]$ and perpendicular $[I_{\perp}(t)]$ to the exciting laser light was detected by two photomultiplier tubes (H5783-01, Hamamatsu Photonics Deutschland GmbH, Herrsching, Germany). The signals from these photomultipliers were collected by a router (NRT 400, PicoQuant GmbH) synchronized with the laser pulses and fed to a time-correlated single photon counting device (TimeHarp 200, PicoQuant GmbH). In addition, unpolarized fluorescence $I(t) = I_{\parallel}(t) + 2I_{\perp}(t)$ was calculated and further evaluated. The whole equipment consisting of lenses, beamsplitter, and photomultipliers could be moved on a programmable scanning table and positioned below each cavity of the microtiter plate. The two photomultipliers were tuned for identical sensitivities in the two detection paths, i.e., deviations from 50:50 beamsplitting were been compensated electronically. A test experiment with polarized laser light showed that cross detection of the "wrong" polarization was below 4% for both photomultipliers.

Unpolarized fluorescence decay curves $I(t)$ were fitted as a sum of exponential terms with reconvolution by the instrumental response function (IRF) corresponding to

$$I(t) = \int_{-\infty}^{t} IRF(t') \sum_i A_i \exp -(t-t')/\tau_i dt', \qquad (2)$$

with fluorescence lifetimes τ_i and pre-exponential factors A_i representing the fractional contributions of the component i. The decay parameters were iteratively recovered with a nonlinear least-squares error minimization based on the Levenberg-Marquardt algorithm.[12] The reduced χ^2 ratios and their autocorrelation functions were used to facilitate the assessment of the fit quality. In addition, the weighted residuals—corresponding to the deviations between measured and fitted values (divided by the square root of photon counts)—were calculated.

Moreover, the anisotropy function $r(t)$ was calculated from fluorescence intensities parallel $[I_{\parallel}(t)]$ and perpendicular $[I_{\perp}(t)]$ to the exciting electric field vector according to

$$r(t) = \frac{I_{\parallel}(t) - I_{\perp}(t)}{I_{\parallel}(t) + 2I_{\perp}(t)}. \quad (3)$$

$r(t)$ was again fitted as a sum of exponential components according to

$$r(t) = \sum_i R_i \exp(-t/\tau_{r,i}), \quad (4)$$

where $\tau_{r,i}$ corresponds to the rotational relaxation times (with respect to different molecular axes), and R_i corresponds to the initial anisotropy of each component. Since in the present case multiexponential curve fitting did not improve the quality of the fit, the evaluation algorithm described by Eq. (4) was reduced to monoexponential curve fitting according to $r(t)=R_0 \exp(-t/\tau_r)$.

For a comparison of fluorescence lifetimes and rotational diffusion times of whole cells (upon epiillumination) and plasma membranes (upon TIR illumination), a fluorescence microscope was used as described elsewhere.[3,4]

3 Results

3.1 *Fluorescence Lifetime Screening*

For validation of the HCS system, time-correlated fluorescence of individual samples with about 2000 cells each was registered in unpolarized and polarized mode. Unpolarized fluorescence decay kinetics are depicted in Fig. 2(a) for U373-MG glioblastoma cells incubated with NBD-cholesterol as well as for T47D-eYFP-Mem transfectants expressing a membrane-associating fluorescent protein. The IRF of a cavity without any cells (also depicted in Fig. 2(a)) served as a control and was used for reconvolution fitting. Fluorescence decay curves were fairly biexponential, and corresponding fitting curves as well as weighted residuals are included in Fig. 2(a) and 2(b).

The parameters (A_i, τ_i) obtained from biexponential curve fitting (with reconvolution) are summarized in Table 1. Values represent medians and median absolute deviations (MADs) of 40 individual measurements from different samples of the microtiter plate. The amplitude of the short-lived component was similar (NBD-cholesterol) or about 3 times lower (EYFP-Mem) than that of the long-lived component. The low MAD values demonstrate that the fluorescence lifetimes of individual samples are highly reproducible. The longer fluorescence lifetime of NBD-cholesterol in U373-MG cells was about twice as high as that measured for NBD-cholesterol solutions (with $\tau_1=7.27\pm0.07$ ns versus $\tau_1=3.47\pm0.04$ ns), whereas the shorter fluorescence lifetime was virtually the same ($\tau_2=1.60\pm0.04$ ns in cells versus 1.56 ± 0.03 ns in solution). Additional measurements in a fluorescence microscope proved that fluorescence lifetimes of whole cells (upon epiillumination) and plasma membranes (upon TIR illumination) differed by less than 10%.

3.2 *Fluorescence Anisotropy Screening*

Fluorescence kinetics $I_{\parallel}(t)$ and $I_{\perp}(t)$ (polarized) as well as $I(t)=I_{\parallel}(t)+2I_{\perp}(t)$ (unpolarized) of T47D-EYFP-Mem cells are depicted in Fig. 3. $I_{\parallel}(t)$ and $I_{\perp}(t)$ result from both fluorescence decay and rotational diffusion. The anisotropy functions $r(t)$ calculated from Eq. (3) for T47D-EYFP-Mem cells and U373-MG glioblastoma cells incubated with NBD-cholesterol are depicted in Fig. 4(a). Both anisotropy curves decrease monotonously from an initial value R_0 and are fitted as monoexponential functions (also depicted in Fig. 4(a)), resulting in a rotational relaxation time $\tau_r=7.88\pm0.81$ ns, an initial anisotropy $R_0=0.275\pm0.019$, and $\chi^2=1.026$ for U373-MG glioblastoma cells incubated with NBD-cholesterol

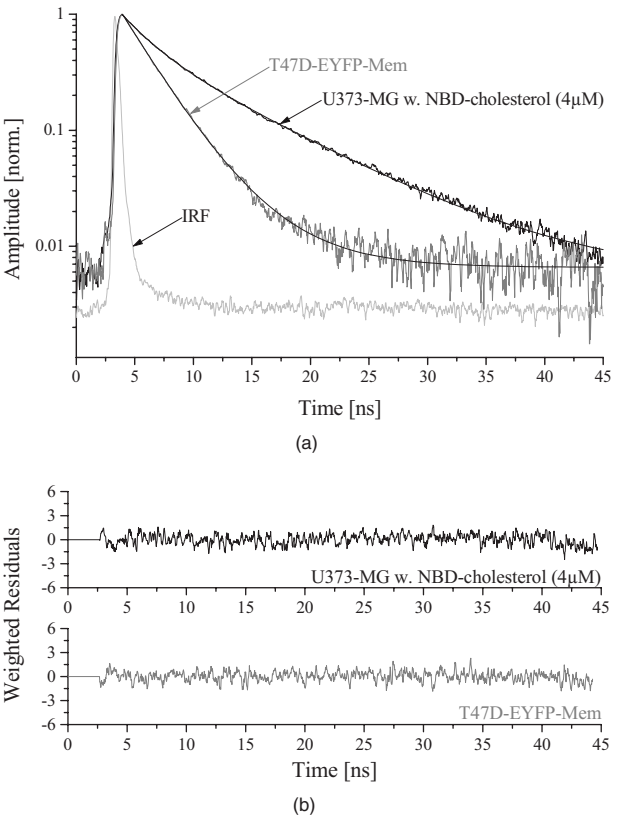

Fig. 2 Normalized fluorescence intensity $I(t)$ of U373-MG glioblastoma cells incubated with NBD-cholesterol (4 μM, 60 min) and of stably transfected T47D-EYFP-Mem breast cancer cells including biexponential fitting curves and IRF (a) with weighted residuals (b). Excitation wavelength: 470 nm; detection range: $\lambda \geqslant 515$ nm.

Table 1 Lifetimes τ_i and normalized amplitudes A_i of membrane-associated fluorescence of U373-MG glioblastoma cells incubated with NBD-cholesterol (4 μM, 60 min), and of T47D-EYFP-Mem cells (excitation wavelength: 470 nm; detection range: $\lambda \geqslant 515$ nm.) Values represent medians and MADs of 40 individual samples of the microtiter plate in each case.

Parameter	U373-MG with NBD-cholesterol (4 μM)	T47D-EYFP-Mem
A_1 [normalized]	0.52	0.75
τ_1 [ns]	7.27 (±0.07)	2.89 (±0.04)
A_2 [normalized]	0.48	0.25
τ_2 [ns]	1.60 (±0.04)	0.93 (±0.11)
χ^2	3.04	1.42

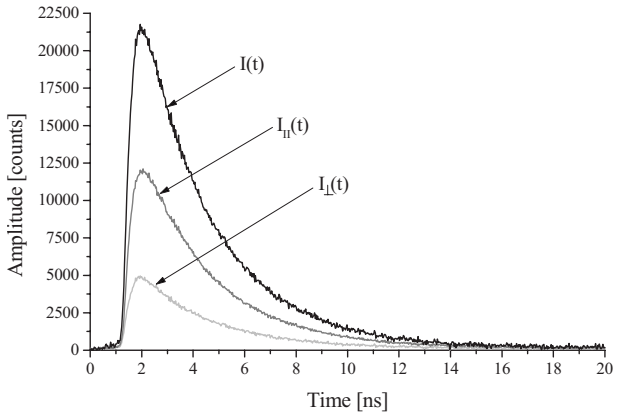

Fig. 3 Fluorescence intensities $I_{\parallel}(t)$, $I_{\perp}(t)$, and $I(t)=I_{\parallel}(t)+2I_{\perp}(t)$ of stably transfected T47D-EYFP-Mem breast cancer cells. Excitation wavelength: 470 nm; detection range: $\lambda \geqslant 515$ nm.

as well as $\tau_r=6.17\pm0.26$ ns, $R_0=0.348\pm0.020$, and $\chi^2=1.439$ for T47D-EYFP-Mem cells. Values represent medians ± MADs of 20 individual samples in each case. χ^2 values as well as the weighted residuals depicted in Fig. 4(b) indicate a rather good exponential fit for NBD-cholesterol and some deviations from the monoexponential behavior for EYFP-Mem. Rotational relaxation times of NBD-cholesterol in U373-MG cells exceeded those measured for NBD-cholesterol solutions ($\tau_r=3.55\pm0.07$) ns by a factor of 2.3, and the initial anisotropy R_0 was considerably higher in glioblastoma cells (0.275) than in solution (0.17). Again, the values of rotational relaxation times of whole cells and plasma membranes differed by less than 10% when measured in the fluorescence microscope.

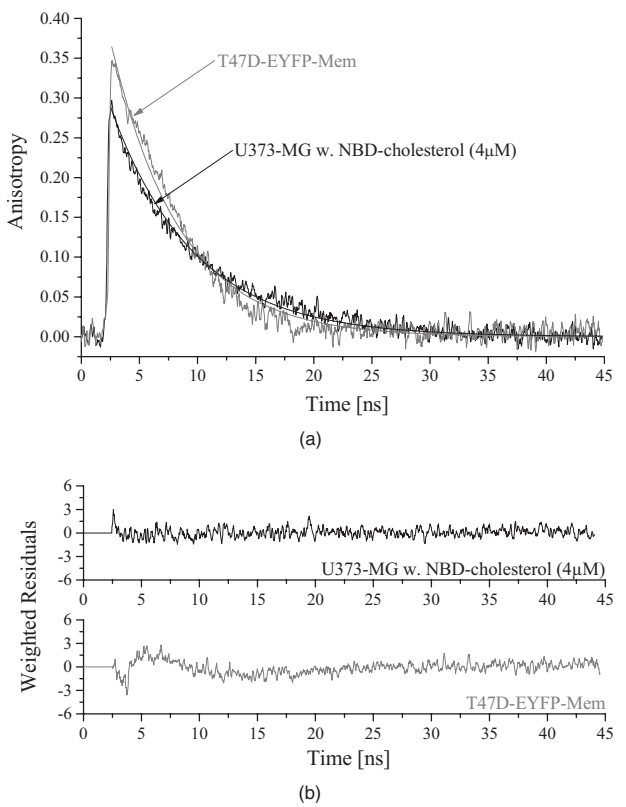

Fig. 4 Anisotropy functions $r(t)$ of stably transfected T47D-EYFP-Mem breast cancer cells and U373-MG glioblastoma cells incubated with NBD-cholesterol (4 μM, 60 min) including monoexponential fitting curves (a) and weighted residuals (b). Excitation wavelength: 470 nm; detection range: $\lambda \geqslant 515$ nm.

4 Discussion

A HCS system for the parameters fluorescence lifetime and fluorescence anisotropy was established with TIR excitation. The system was validated with cultivated cells either incubated with a fluorescent membrane marker or expressing a membrane-associating fluorescent protein. Highly reproducible fluorescence lifetimes and rotational diffusion times were measured for a large number of samples. Therefore, plasma membrane-associated parameters, e.g., membrane fluidity or protein dynamics, were measured reliably. In addition, the HCS system was combined with an existing TIR fluorescence reader[11] so that a larger number of samples could be screened rapidly, whereas a smaller number of selected samples was examined in detail for fluorescence lifetime and anisotropy parameters.

Fluorescence decay curves of NBD-cholesterol in U373-MG cells and T47D-EYFP-Mem cells showed biexponential behavior, indicating that different molecular conformations or locations of the fluorophores might coexist. This seems to be similar in the plasma membrane and in intracellular membranes, since fluorescence lifetimes were almost identical upon TIR and epiillumination. However, the longer fluorescence lifetime of NBD-cholesterol in solution is smaller by a factor 2 than cell measurements, which again demonstrates the important role of its microenvironment. For NBD-cholesterol and T47D-EYFP-Mem cells, the relative fluorescence intensity—corresponding to the normalized product of relative amplitude and fluorescence lifetime $A_2\tau_2/(A_1\tau_1+A_2\tau_2)$ of the short-lived component—was comparably small. This may explain why only one rotational diffusion time could be resolved in each case. Rotational diffusion times of NBD-cholesterol in U373-MG cells and T47D-EYFP-Mem cells were similar, but it was only in the case of NBD-cholesterol that the clear monoexponential behavior of $r(t)$ indicated rather free molecular rotation. In the case of EYFP-Mem, deviations from this monoexponential behavior may have resulted from some restriction in molecular rotation due to membrane binding. However, tentative fitting by a 2-D (in-plane) rotation model[13] did not improve the quality of the fit and increased the χ^2 values in comparison with the model of free (3-D) molecular rotation described by Eq. (3). So far, there is no experimental evidence that Förster resonance energy transfer between fluorophores of the same species (homo-FRET)[14] might here affected fluorescence anisotropy in the cell cultures. However, due to the smaller value R_0 measured for NBD-cholesterol solutions, homo-FRET (occurring, e.g., in aggregated dye molecules) cannot be excluded. The initial anisotropy R_0 mainly reflects the angle β between optical excitation and emission dipoles of the fluorophores, which according to the relation[15]

$$R_0 = \frac{2}{5}\left(\frac{3\cos^2\beta - 1}{2}\right) \quad (5)$$

is about 17 deg for EYFP-Mem and 27 deg for intracellular NBD-cholesterol.

TIR measurements of fluorescence anisotropy may contribute largely to studies of membrane dynamics of living cells. Presently, membrane stiffness and fluidity are investigated as a function of temperature, cell age, and intracellular amounts of cholesterol.[4,16] Changes in cholesterol amounts in cell membranes have been related to various diseases[17–19] and may have some influence on the uptake of pharmaceutical agents. Therefore, in the future fluorescence anisotropy screening using TIR illumination may also have some potential for clinical studies.

Acknowledgments

This project was supported by the Ministerium für Wissenschaft, Forschung und Kunst Baden-Württemberg, Germany. Technical assistance by Claudia Hintze is gratefully acknowledged.

References

1. D. Axelrod, "Cell-substrate contacts illuminated by total internal reflection fluorescence," *J. Cell Biol.* **89**, 141–145 (1981).
2. G. A. Truskey, J. S. Burmeister, E. Grapa, and W. M. Reichert, "Total internal reflection fluorescence microscopy (TIRFM) (II) topographical mapping of relative cell/substratum separation distances," *J. Cell. Sci.* **103**, 491–499 (1992).
3. K. Stock, R. Sailer, W. S. L. Strauss, M. Lyttek, R. Steiner, and H. Schneckenburger, "Variable-angle total internal reflection fluorescence microscopy (VA-TIRFM): realization and application of a compact illumination device," *J. Microsc.* **211**, 19–29 (2003).
4. H. Schneckenburger, M. Wagner, M. Kretzschmar, W. S. L. Strauss, and R. Sailer, "Laser-assisted fluorescence microscopy for measuring cell membrane dynamics," *Photochem. Photobiol. Sci.* **3**, 817–822 (2004).
5. E. Sund and D. Axelrod, "Actin dynamics at the living cell submembrane imaged by total internal fluorescence photobleaching," *Biophys. J.* **79**, 1655–1669 (2000).
6. G. M. Omann and D. Axelrod, "Membrane-proximal calcium transients in stimulated neutrophils detected by total internal reflection fluorescence," *Biophys. J.* **71**, 2885–2891 (1996).
7. A. Demuro and I. Parker, "Imaging the activity and localization of single voltage-gated Ca^{2+} channels by total internal reflection fluorescence microscopy," *Biophys. J.* **86**, 3250–3259 (2004).
8. W. J. Betz, F. Mao, and C. B. Smith, "Imaging exocytosis and endocytosis," *Curr. Opin. Neurobiol.* **6**, 365–371 (1996).
9. M. Oheim, D. Loerke, W. Stuehmer, and R. H. Chow, "The last few milliseconds in the life of a secretory granule," *Eur. Biophys. J.* **27**, 83–98 (1998).
10. V. Beaumont, "Visualizing membrane trafficking using total internal reflection fluorescence microscopy," *Biochem. Soc. Trans.* **31**, 819–823 (2003).
11. T. Bruns, W. S. L. Strauss, R. Sailer, M. Wagner, and H. Schneckenburger, "Total internal reflectance fluorescence reader for selective investigations of cell membranes," *J. Biomed. Opt.* **11**, 034011 (2006).
12. D. V. O'Connor and D. Philipps, *Time-Correlated Single Photon Counting*, Academic Press, London (1984).
13. M. L. Gee, L. Lenson, T. A. Smith, and C. A. Scholes, "Time-resolved evanescent wave induced fluorescence anisotropy for the determination of molecular conformational changes of proteins at an interface," *Eur. Biophys. J.* **33**, 130–139 (2004).
14. E. K. L. Yeow and A. H. A. Clayton, "Enumeration of oligomerization states of membrane proteins in living cells by homo-FRET spectroscopy and microscopy: theory and application," *Biophys. J.* **92**, 3098–3104 (2007).
15. J. R. Lakowicz, *Principles of Fluorescence Spectroscopy*, 3rd edition, Springer Science + Business, New York (2006).
16. P. Weber, M. Wagner, and H. Schneckenburger, "Microfluorometry of cell membrane dynamics," *Cytometry* **69A**, 185–188 (2006).
17. G. P. Eckert, N. J. Cairns, A. Maras, W. F. Gattaz, and W. E. Muller, "Cholesterol modulates the membrane-disordering effects of beta-amloyid peptides in the hippocampus: specific changes in Alzheimer's disease," *Dementia Geriatr. Cognit. Disord.* **11**, 181–186 (2000).
18. S. Aozaki, "Decreased membrane fluidity in erythrocytes from patients with Crohn's disease," *Gastroenterol. Jpn.* **24**, 246–254 (1989).
19. T. Koike, G. Ishida, M. Taniguchi, K. Higaki, Y. Ayaki, M. Saito, Y. Sakakihara, Y. Iwamori, and K. Onno, "Decreased membrane fluidity and unsaturated fatty acids in Niemann-Pick disease type C fibroblasts," *Biochim. Biophys. Acta* **1406**, 327–335 (1998).